Effects of macro-scale bed roughness geometry on flow resistance

Effects of macro-scale bed roughness geometry on flow resistance

F. Canovaro,[1,2] E. Paris,[1] and L. Solari[1]

Received 13 November 2006; revised 9 May 2007; accepted 21 May 2007; published 12 October 2007.

[1] Flow field over macro-roughness elements, as, for example, in flow conditions such as of steep mountain streams, is investigated by means of a theoretical model and a laboratory study with the main aim of understanding the influence of concentration and planimetric disposition of grain roughness on flow resistance. A theoretical model for the average velocity distribution profile over a bed with macro-roughness elements is developed herein. The model is based on a two-layer approach which takes into account the displacement of the main flow due to the drag around the roughness. The laboratory study is composed of an extensive set of flume experiments in the case of steep slopes and large relative roughness conditions. For a given flow discharge and bed slope, various experiments have been carried out with different patterns and spacing of the roughness elements constituted by river pebbles. Application of the theoretical model to the experimental results enables the determination of how flow resistance is affected by the macro-roughness; in particular, it appears that when the concentration of the roughness is within an optimal range, flow resistance is maximum.

Citation: Canovaro, F., E. Paris, and L. Solari (2007), Effects of macro-scale bed roughness geometry on flow resistance, *Water Resour. Res.*, *43*, W10414, doi:10.1029/2006WR005727.

1. Introduction

[2] Flows over macro-scale roughness can be easily found in nature, such as in mountain streams [*Bathurst*, 1985], overland flows [*Lawrence*, 2000] and inundation of floodplains [*Järvelä*, 2002]. In the case of mountain streams, due to the presence of large rocks and boulders protruding from the steep channel bed, the flow depth is typically comparable with roughness size. In these conditions, clasts protruding from the channel bed interfere with the flow, and a drag force is exerted on these obstructions, causing a local reduction of the flow momentum. If the number of macro-roughness elements interacting with the lower portion of the flow is considerable, the assumption of a logarithmic velocity profile is no longer valid, and the classical expression of flow resistance formulae cannot be applied [*Bathurst*, 1987]. Field and laboratory measurements of velocity profiles in high gradient gravel bed streams [*Marchand et al.*, 1984; *Baiamonte et al.*, 1995; *Bathurst*, 1987] suggest that the velocity takes an "S-shaped" profile and at least two flow regions can be identified in the flow field: a near bed region characterized by relatively low flow velocity dominated by the loss of flow momentum due to drag around the bed material and an upper region, in proximity to the water surface, characterized by significantly higher velocities distributed according to a profile which deviates from a logarithmic law (see *Katul et al.* [2002] for a mixing layer theory application to such flow field profile). Notwithstanding such observations, the majority of the formulae employed to estimate flow resistance are of the logarithmic type using a single representative roughness scale (see *Bettess* [1999] for a review and comparison of flow resistance equations for gravel bed rivers). On the other hand, previous analyses [e.g., *Hey*, 1979; *Bathurst et al.*, 1981; *Pyle and Novak*, 1981; *Bathurst*, 1985; *Aguirre-Pe and Fuentes*, 1990; *Baiamonte et al.*, 1995; *Nikora et al.*, 1998; *Ferro*, 1999; *Aberle and Smart*, 2003] suggest that, in case of macro-scale roughness, the flow velocity profile and, therefore, the flow resistance are a function not only of the relative submergence (defined as the ratio of mean flow depth Y to a characteristic grain diameter D) but also of additional parameters related to the "roughness geometry", such as spatial density and arrangement of macro-roughness elements. In particular, *Ferro and Giordano* [1993] suggest, in case of no vegetation, the following functional relationship for dimensionless Chezy coefficient:

$$C = \sqrt{\frac{8}{f}} = fn(Re, Fr, Y/D, \Gamma, P_1, P_2, \tau^*) \qquad (1)$$

where f is the Darcy-Weisbach friction factor, Re and Fr are flow Reynolds and Froude numbers, Y/D is relative submergence, Γ is macro-roughness spatial density, P_1 and P_2 are two parameters related to the macro-roughness planimetric arrangement (for example, a characteristic longitudinal and transversal distance) between the macro-roughness elements, and τ^* is the Shields parameter. The influence on flow resistance played by Re, Fr, Y/D, and τ^* in the case of mountain streams has been already investigated by several authors [e.g., *Bathurst et al.*, 1981; *Graf*, 1984; *Colosimo et al.*, 1988; *Baiamonte et al.*, 1995;

[1]Department of Civil and Environmental Engineering, University of Firenze, Firenze, Italy.
[2]Now at CERAFRI (Centre of Research and Advanced education for Hydrogeological Risk Prevention), Retignano di Stazzema (LU), Italy.

0043-1397/07/2006WR005727$09.00

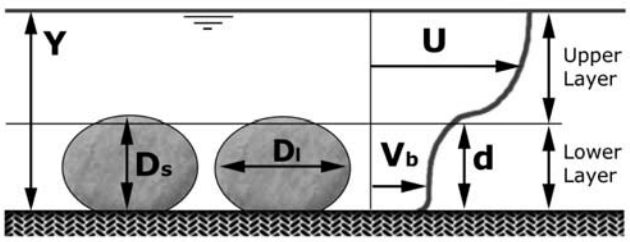

Figure 1. Sketch of the flow field in the streamwise direction and notations.

Ferro, 1999]; while the role played by macro-roughness spatial density and pattern arrangement does not appear to be completely clarified, even if various authors have pointed out their importance [*Rouse*, 1965; *Hey*, 1979; *Nowell and Church*, 1979; *Bathurst et al.*, 1981; *Pyle and Novak*, 1981; *Baiamonte et al.*, 1995; *Ferro*, 1999]. In particular, the pioneering contribution of *Rouse* [1965], in the case of regular dispositions of uniform and artificial roughness, indicates the existence of an optimum value of spatial density which produces the maximum of flow resistance.

[3] In the present work, average flow field over a bed with macro-scale roughness is investigated with the aim of understanding how flow resistance is influenced by macro-roughness spatial density and planimetric arrangement. The problem is tackled by means of a theoretical model, which predicts the average flow field when the flow depth is of the same order as the roughness size and of an extensive laboratory experimental activity with different hydraulic and macro-roughness conditions.

2. Theoretical Model

[4] A theoretical model of the average flow field is herein developed. Let us consider the steady flow and spatially averaged uniform conditions with the channel bed covered by macro-roughness elements represented by fluvial clasts and no sediment transport. The entire flow field of depth Y is assumed to be composed by two layers (Figure 1):

[5] 1. a *lower layer*, lying on the bed and containing the major part of macro-roughness elements, in which the flow is slowed by the loss of momentum due to the drag around the obstacles. In such layer of thickness d, the flow velocity among the roughness V_b is relatively low and approximately constant through the depth.

[6] 2. An *upper layer* of height $Y - d$, extending up to the free surface, where the major part of the discharge occurs with a relatively high average flow velocity U.

[7] For a control volume of unit bed area extending from the bed to the water surface, water continuity equation and momentum balance equation in the streamwise direction give:

$$\begin{cases} q = (Y-d)U + d\psi V_b \\ \tau_g = \tau_d + \tau_s. \end{cases} \quad (2)$$

Table 1. Mean Geometrical Properties of Employed Pebbles

Set of Pebbles	Φ, –	D_s, cm	D_m, cm	D_l, cm	V, cm^3	N_u^{max}, –
1	−5.25	2.6	3.8	5.5	29	575
2	−5.75	4.3	5.4	8	96	290
3	−6.25	5.7	7.6	9.8	223	145

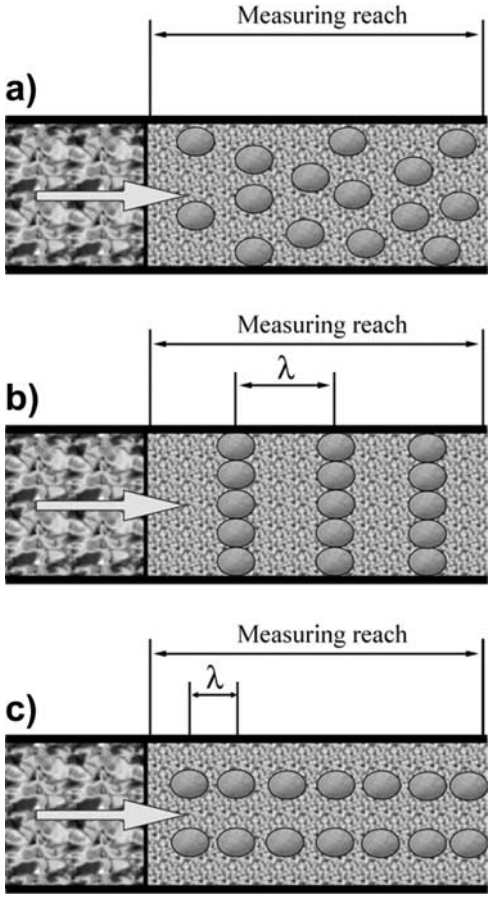

Figure 2. Sketches of the planimetric arrangements of the macro-roughness: *Random pattern* (a), *Transversal stripe pattern* (b), and *Longitudinal stripe pattern* (c).

where q is the discharge per unit width, τ_g is the global shear stress, due to the streamwise water mass weight, τ_d is the drag shear stress, related to the macro-roughness-induced drag force, τ_s is the surface shear stress, related to the surface-induced friction force, and ψ is a reduction coefficient for the lower layer effective flow velocity V_b, depending on the effective cross-sectional area among the macro-roughness elements occupied by the flow. Therefore, ψV_b denotes the apparent average flow velocity in the lower layer, as if no obstacles would be present.

[8] Note that ψ is always smaller than 1, being defined as the ratio between the cross-sectional area occupied by the

Table 2. Summary of Experimental Series Carried out Employing *Random Pattern*

Experimental Series	Runs Number	Q, l/s	S, %	Φ, –
Random I	18	7.3	2.5	−5.25
Random II	18	7.3	0.5	−5.75
Random III	18	4.0	1.0	−5.75
Random IV	18	7.3	1.0	−5.75
Random V	18	10.0	1.0	−5.75
Random VI	18	13.5	1.0	−5.75
Random VII	18	16.0	1.0	−5.75
Random VIII	18	7.3	1.5	−5.75
Random IX	18	7.3	2.0	−5.75
Random X	18	7.3	2.5	−5.75
Random XI	9	7.3	2.5	−6.25

Table 3. Summary of Experimental Series Carried out Employing Transversal Stripe Pattern

Experimental Series	Runs Number	q, l/s	S, %	Φ, –	λ, cm
TrStripes I	10	7.3	2.5	−5.25	10–60
TrStripes II	9	7.3	1.0	−5.75	15–80
TrStripes III	8	13.5	1.0	−5.75	15–80
TrStripes IV	11	7.3	2.5	−5.75	10–80
TrStripes V	9	13.5	1.0	−6.25	8–160
TrStripes VI	9	4.7	2.5	−5.75	8–160
TrStripes VII	9	7.3	2.5	−5.75	8–160
TrStripes VIII	9	4.7	3.0	−5.75	8–160
TrStripes IX	9	7.3	3.0	−5.75	8–160
TrStripes X	9	8.2	3.0	−5.75	8–160
TrStripes XI	9	5.2	4.0	−5.75	8–160
TrStripes XII	9	6.4	4.0	−5.75	8–160
TrStripes XIII	9	7.3	4.0	−5.75	8–160
TrStripes XIV	9	8.2	4.0	−5.75	8–160
TrStripes XV	7	6.4	6.0	−5.75	8–160
TrStripes XVI	6	7.3	6.0	−5.75	8–160
TrStripes XVII	6	8.2	6.0	−5.75	8–160
TrStripes XVIII	8	13.5	0.2	−5.25	15–80
TrStripes XIX	9	13.5	0.2	−5.75	20–100
TrStripes XX	9	13.5	0.2	−6.25	15–100

flow among the macro-roughness elements in the lower layer and the total cross-sectional area of the lower layer. Generally, ψ is a function of both the number and the planimetric arrangement of macro-roughness. In the case of a random planimetric arrangement with the macro-roughness placed with the short axis perpendicular to the channel bed and the long axis parallel the channel axis, ψ can be estimated as:

$$\psi = \begin{cases} 1 - \frac{\pi}{4} D_m \sqrt{N_u} & \text{if } d \le D_s \\ 1 - \frac{\pi}{4} \frac{D_s}{d} D_m \sqrt{N_u} & \text{if } d > D_s. \end{cases} \quad (3)$$

where D_s and D_m are the short and median axis diameters of the macro-roughness elements, approximated with ellipsoids, and N_u is the number of macro-roughness elements arranged on an unit bed area. The calculations leading to the expression of ψ reported in equation (3) can be found in Appendix A.

[9] The global shear stress per unit bed area involved in the second equation of system (2) is expressed as follows:

$$\tau_g = \rho g Y S \left(1 - \frac{2 D_s G}{3 Y}\right) \quad (4)$$

where ρ is the water density, g is the gravitational acceleration, S is the channel slope, and Γ is the macro-roughness spatial density, defined as the ratio between the number of macro-roughness elements per unit bed area, and the maximum number that is possible to arrange in the same area: $\Gamma = N_u/N_u^{max}$. The term into brackets acts as a reduction factor, in order to exclude from calculations the control volume fraction occupied by macro-roughness elements. The calculations leading to the expression of τ_g in (4) are given in Appendix B.

[10] According to the two-layer scheme, each macro-roughness element in the lower layer is subject to a drag force due to the flow impacting on it. The overall effect of the macro-roughness elements on the flow can be estimated writing the total drag force per unit bed area as follows:

$$\tau_d = \frac{1}{2} \rho C_d N_u A_f V_b^2 \quad (5)$$

where A_f is the cross-sectional impact area of a single macro-roughness element and C_d is a drag coefficient, here assumed to be constant and equal to 1.5 as suggested by *Roberson et al.* [1974] and *Bathurst* [1996] in the case of natural boulders.

[11] Finally, force per unit bed area due to skin friction takes the following expression:

$$\tau_s = \rho U^2 \left[\frac{(1-\Gamma)}{C_G^2} + \frac{\Gamma}{C_P^2}\right] \quad (6)$$

being C_G the Chezy coefficient associated to the base material beneath the boulders (estimated at $\Gamma = 0$) and C_P is the Chezy coefficient associated to the boulder skin friction (estimated at $\Gamma = 1$).

[12] According to the two-layer approach described above, the average flow quantities are the total water depth (Y), the upper layer average flow velocity (U), the lower layer thickness (d), and the lower layer flow velocity (V_b). In the present work, the governing equations (2) are solved for the unknowns d and V_b, given Y and U.

[13] Once the average flow velocity profile is obtained, the mean flow velocity $\overline{U}$ can be estimated as a weighted average of the flow velocities in the upper and bottom layers with weights equal to the flow discharges in the upper and bottom layers and reads:

$$\overline{U} = \frac{(Y-d)U^2 + d(\psi V_b)^2}{q} \quad (7)$$

Such definition of mean velocity $\overline{U}$ is consistent with the definition of the flow depth Y which is always measured from the granular layer. When the bed is completely covered by the macro-roughness, V_b is very low, and d is comparable with D_s; in this condition, the mean flow velocity $\overline{U}$ is similar to U; a classical depth-averaged value of the flow velocity would lead instead to an unrealistic mean value much smaller than U.

[14] Finally, the average dimensionless Chezy coefficient C can be evaluated as follows:

$$C = \frac{\overline{U}}{\sqrt{\tau_g/\rho}} \quad (8)$$

3. Laboratory Experiments

3.1. Setup

[15] Experiments were carried out in a 10-m-long, 36.5-cm-wide and 50-cm-deep glass-walled recirculating tilting

Table 4. Summary of Experimental Series Carried out Employing Longitudinal Stripe Pattern

Experimental Series	Runs Number	Q, l/s	S, %	Φ, –
LonStripes I	9	7.3	2.5	−5.25
LonStripes II	9	7.3	1.0	−5.75
LonStripes III	8	13.5	1.0	−5.75
LonStripes IV	8	7.3	2.5	−5.75

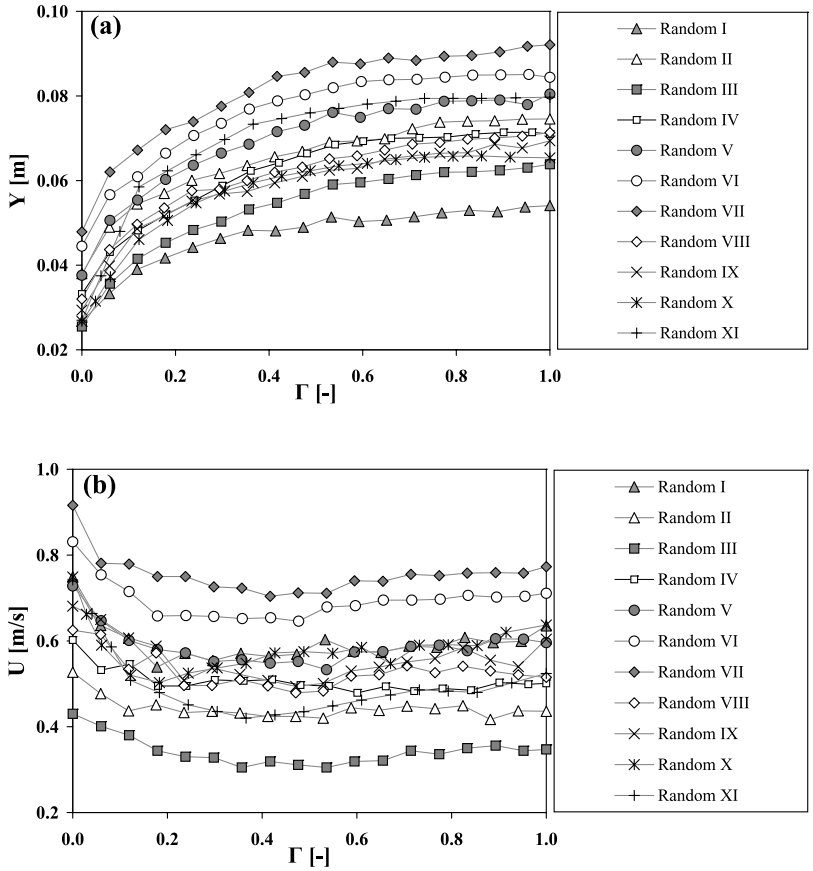

Figure 3. Total water depth (Y) (a) and upper layer flow velocity (U) (b) as functions of spatial density (Γ), in case of *Random pattern*.

flume (Hydraulic Laboratory of the Civil Engineering Department of Firenze University). The 4-m-long measuring reach, composed by a 8-cm-thick layer of a rather uniform granular material of 7 mm in diameter, was located at about 5 m from the flume entrance section. A 1.5-m-long reach of quarry rubbles was positioned before the beginning of the measuring reach to avoid large-scale disturbance in the reach under investigation. The recirculating water discharge was regulated by a valve and measured by means of an electromagnetic flowmeter. All the experiments were carried out in the case of fixed-bed conditions and average uniform and stationary conditions.

[16] Total water depth Y was measured by means of a set of 19 piezometers placed under the granular layer. During each experimental run, piezometers were read twice (a time interval of 15 minutes was observed between the readings) obtaining 38 water depth readings along the whole measuring reach; those values were referred to the mean level of the granular layer surface. Measured values were then averaged in space and time to obtain a single averaged water depth value for each experimental run.

[17] Averaged upper layer flow velocity U was measured by means of a micro-propeller current meter of about 15-mm diameter. Twenty-seven measurement points were employed along the measuring reach at 9 cross-sections at a relative distance of 50 cm; in each cross-section, the velocity was taken symmetrically with respect to the channel axis. Since the thickness of the lower layer d was not known during the experiments, the upper layer flow velocity U was measured in proximity of the water surface at about the 80% of the depth from the bed; just one measurement was taken along each vertical since preliminary measurements showed that the velocity profile was very flat over the macro-roughness, at least employing the micro-propeller. This approximation is also confirmed by some authors [*Carollo et al.*, 2002; *Stone and Shen*, 2002] who measured a very flat velocity profile over a vegetated bed. Notwithstanding the differences between a vegetated bed and a bed with protruding boulders, it seems reasonable that both behave as macro-roughness elements.

[18] River pebbles were employed as macro-roughness elements. The pebbles were placed above the granular layer with the short axis perpendicular to granular layer [*Zimmermann and Church*, 2001] and the long axis parallel to the channel axis; this orientation is partly in agreement with what is normally found in streams where the stones tend to have the longitudinal axis perpendicular to the flow direction.

[19] Three different sets of pebbles were employed, characterized by a median axis dimension of $\Phi = -5.25$ (32–45 mm sieve fraction), $\Phi = -5.75$ (45–64 mm sieve fraction) and $\Phi = -6.25$ (64–90 mm sieve fraction), where Φ is the Wentworth sedimentological scale according to which $\Phi = -\log_2(D_m)$, with D_m in [mm] units; the main characteristics of the employed pebbles are in Table 1. Experiments were carried out varying flow discharge, flume slope, and pebble size. The pebble spatial density was varied from 0 to 1 in the case of three different planimetric

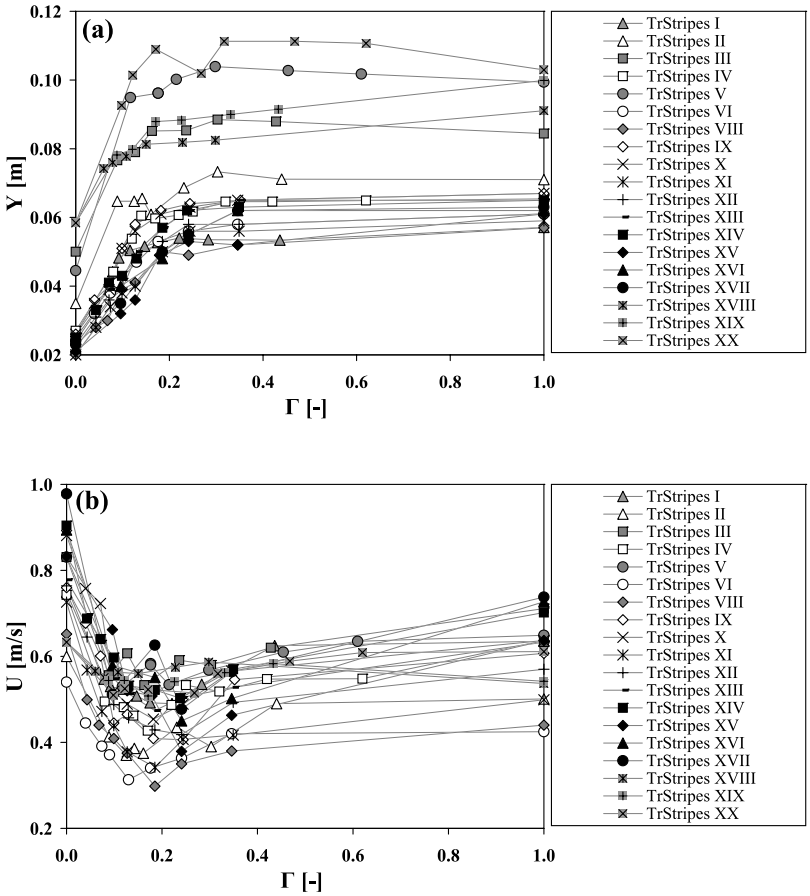

Figure 4. Total water depth (Y) (a) and upper layer flow velocity (U) (b) as functions of spatial density (Γ), in the case of *Transverse Stripe pattern*.

arrangements, here called "*Random pattern*," "*Transversal stripe pattern*," and "*Longitudinal stripe pattern*".

[20] As shown in Figure 2a, *Random pattern* refers to an irregular random-like planimetric arrangement of macro-roughness elements; this pattern may be thought as a schematic representation of the macro-roughness occurring in a steep mountain streams. This arrangement was obtained filling the flume bed measuring reach completely with pebbles ($\Gamma = 1$) and then randomly removing a fixed number of pebbles at each experimental run, until no macro-roughness elements were present ($\Gamma = 0$). A total of 189 runs were carried out for this pattern (see Table 2).

[21] *Transversal stripe pattern* refers to a streamwise sequence of transversal macro-roughness stripes placed along the channel (Figure 2b); this pattern may be thought as representative of a step-pool like morphology. In this arrangement, the distance or wavelength λ between the stripes was varied from a minimum value, when the stripes are in contact with each other, to a maximum value corresponding to a negligible spatial density.

[22] The reduction coefficient ψ in this case reads (see also Appendix A):

$$\psi = \begin{cases} 1 - \dfrac{D_l}{\lambda} & \text{if } d \le D_s \\ 1 - \dfrac{D_s}{d}\dfrac{D_l}{\lambda} & \text{if } d > D_s. \end{cases} \tag{9}$$

[23] A total of 173 experimental runs were carried out for this pattern (see Table 3).

[24] In the *Longitudinal stripe pattern*, macro-roughness is positioned according to rows parallel to the streamwise direction (Figure 2c). Two longitudinal rows symmetrical to the channel axis have been analyzed varying the spatial density by changing the distance between two consecutive pebbles. The *Longitudinal stripe pattern* does not have any apparent natural counterpart; the reason for using this pattern is to have a more complete understanding of the influence of the planimetric arrangement of the obstacles on the flow resistance.

[25] The reduction coefficient ψ is estimated as follows (see also Appendix A):

$$\psi = \begin{cases} 1 - \dfrac{\pi}{4} D_m N_r \dfrac{D_l}{\lambda} & \text{if } d \le D_s \\ 1 - \dfrac{\pi}{4}\dfrac{D_s}{d} D_m N_r \dfrac{D_l}{\lambda} & \text{if } d > D_s. \end{cases} \tag{10}$$

where N_r is the number of longitudinal stripes.

[26] A total of 34 experimental runs were carried out for this pattern (see Table 4).

[27] Flow appeared to be globally steady and spatially uniform on average along the measuring reach; although locally was, in various configurations, rapidly varying; for instance, in the case of *Transversal stripe pattern* when the

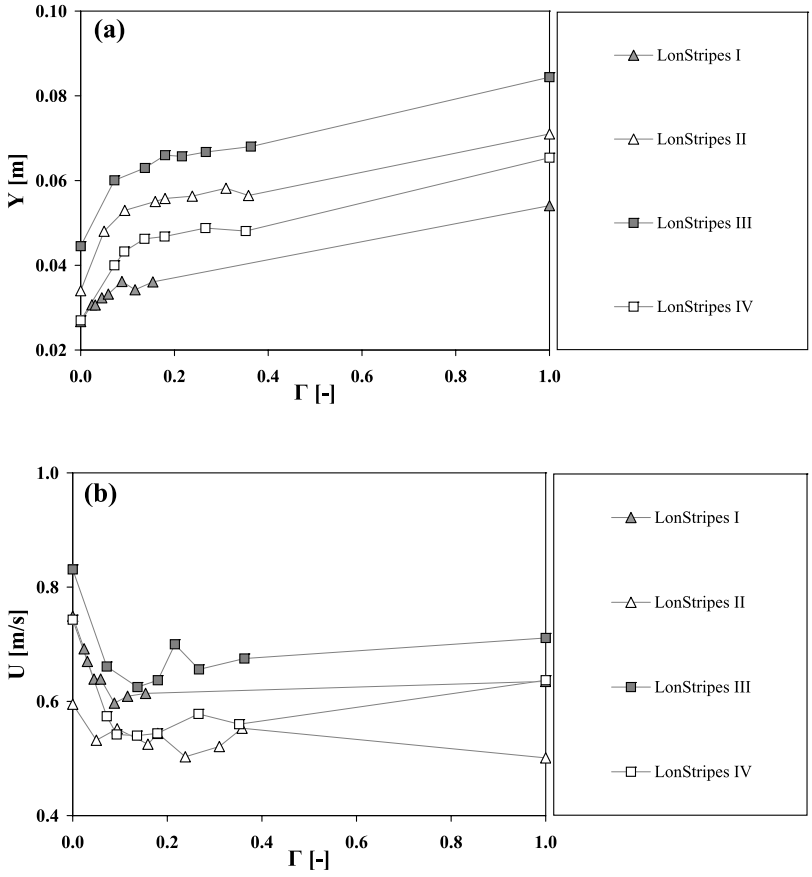

Figure 5. Total water depth (Y) (a) and upper layer flow velocity (U) (b) as functions of spatial density (Γ), in the case of *Longitudinal Stripe pattern*.

bed slope was higher than 2%, the flow was tumbling over each individual step.

3.2. Measured Data

[28] The space-time averaged flow depth Y and upper flow velocity U for all the experiments are shown in Figures 3, 4 and 5 for *Random pattern*, *Transverse stripe pattern*, and *Longitudinal stripe pattern*, respectively. Notwithstanding that the influence on the flow field of the macro-roughness pattern is quantitatively different, some common behavior can be observed. In particular, Figures 3a and 4a show that total water depth Y rapidly increases with Γ at lower spatial density values, and then it becomes asymp-

Table 5. Measured Data for Random I, Random II and Random III Experimental Series

Random I			Random II			Random III		
Γ, –	*Y*, m	*U*, m/s	Γ, –	*Y*, m	*U*, m/s	Γ, –	*Y*, m	*U*, m/s
0.000	0.027	0.749	0.000	0.038	0.527	0.000	0.026	0.430
0.059	0.033	0.636	0.059	0.049	0.477	0.060	0.036	0.401
0.118	0.039	0.606	0.118	0.054	0.437	0.119	0.042	0.380
0.178	0.042	0.539	0.176	0.057	0.451	0.179	0.045	0.344
0.237	0.044	0.571	0.235	0.060	0.433	0.238	0.048	0.330
0.296	0.046	0.554	0.294	0.062	0.436	0.298	0.050	0.328
0.355	0.048	0.571	0.353	0.064	0.432	0.357	0.053	0.305
0.414	0.048	0.564	0.412	0.066	0.424	0.417	0.055	0.319
0.473	0.049	0.569	0.471	0.067	0.424	0.476	0.057	0.311
0.533	0.051	0.603	0.529	0.069	0.420	0.536	0.059	0.305
0.592	0.050	0.576	0.588	0.069	0.444	0.595	0.060	0.319
0.651	0.051	0.573	0.647	0.070	0.438	0.655	0.060	0.321
0.710	0.051	0.588	0.706	0.072	0.448	0.714	0.061	0.344
0.769	0.052	0.585	0.765	0.074	0.442	0.774	0.062	0.336
0.828	0.053	0.608	0.824	0.074	0.449	0.833	0.062	0.350
0.888	0.053	0.596	0.882	0.074	0.417	0.893	0.062	0.356
0.947	0.054	0.599	0.941	0.075	0.437	0.952	0.063	0.344
1.000	0.054	0.635	1.000	0.075	0.436	1.000	0.064	0.347

Table 6. Measured Data for Random IV, Random V, and Random VI Experimental Series

Random IV			Random V			Random VI		
Γ, –	*Y*, m	*U*, m/s	Γ, –	*Y*, m	*U*, m/s	Γ, –	*Y*, m	*U*, m/s
0.000	0.033	0.602	0.000	0.038	0.728	0.000	0.045	0.831
0.060	0.043	0.532	0.060	0.051	0.647	0.060	0.057	0.754
0.120	0.048	0.546	0.119	0.055	0.601	0.119	0.061	0.715
0.180	0.052	0.495	0.179	0.060	0.580	0.179	0.066	0.658
0.240	0.055	0.495	0.238	0.064	0.572	0.239	0.071	0.659
0.300	0.059	0.509	0.298	0.066	0.552	0.298	0.074	0.657
0.361	0.062	0.507	0.357	0.069	0.556	0.358	0.077	0.652
0.421	0.064	0.510	0.417	0.072	0.548	0.418	0.079	0.654
0.481	0.066	0.497	0.476	0.073	0.552	0.477	0.080	0.646
0.541	0.069	0.495	0.536	0.076	0.533	0.537	0.082	0.679
0.601	0.069	0.479	0.595	0.075	0.574	0.597	0.083	0.682
0.661	0.070	0.494	0.655	0.077	0.575	0.656	0.084	0.695
0.721	0.070	0.483	0.714	0.077	0.587	0.716	0.084	0.695
0.781	0.070	0.489	0.774	0.079	0.590	0.776	0.084	0.697
0.841	0.071	0.485	0.833	0.079	0.577	0.835	0.085	0.706
0.901	0.071	0.503	0.893	0.079	0.605	0.895	0.085	0.702
0.962	0.071	0.499	0.952	0.078	0.604	0.955	0.085	0.704
1.000	0.071	0.501	1.000	0.080	0.596	1.000	0.084	0.711

Table 7. Measured Data for Random VII, Random VIII and Random IX Experimental Series

Random VII			Random VIII			Random IX		
Γ, –	*Y*, m	*U*, m/s	Γ, –	*Y*, m	*U*, m/s	Γ, –	*Y*, m	*U*, m/s
0.000	0.048	0.916	0.000	0.032	0.625	0.000	0.029	0.681
0.060	0.062	0.781	0.059	0.044	0.615	0.059	0.040	0.650
0.119	0.067	0.779	0.118	0.050	0.534	0.118	0.049	0.607
0.179	0.072	0.750	0.176	0.054	0.572	0.176	0.052	0.588
0.238	0.074	0.750	0.235	0.058	0.496	0.235	0.055	0.508
0.298	0.078	0.726	0.294	0.058	0.496	0.294	0.057	0.537
0.357	0.081	0.723	0.353	0.060	0.510	0.353	0.057	0.522
0.417	0.085	0.704	0.412	0.062	0.495	0.412	0.059	0.508
0.476	0.086	0.712	0.471	0.063	0.479	0.471	0.061	0.494
0.536	0.088	0.711	0.529	0.065	0.483	0.529	0.062	0.501
0.595	0.088	0.740	0.588	0.066	0.518	0.588	0.063	0.530
0.655	0.089	0.739	0.647	0.067	0.521	0.647	0.065	0.539
0.714	0.088	0.755	0.706	0.069	0.542	0.706	0.066	0.551
0.774	0.089	0.752	0.765	0.069	0.526	0.765	0.066	0.559
0.833	0.090	0.758	0.824	0.070	0.541	0.824	0.067	0.584
0.893	0.090	0.759	0.882	0.070	0.530	0.882	0.069	0.555
0.952	0.092	0.758	0.941	0.071	0.521	0.941	0.068	0.540
1.000	0.092	0.773	1.000	0.071	0.515	1.000	0.069	0.604

totically constant when Γ is approaching 1; the rate of increase is much higher for low values of Γ. In the case of *Longitudinal stripe pattern*, Figure 5a, *Y* increases with Γ without showing any asymptotic behavior; this is probably due to the geometry of this pattern which forced the flow to funnel in the space between the longitudinal stripes. Note that when roughness concentration is high (Γ approaches 1), the influence of the pattern on the flow field vanishes since all the patterns collapse into the same configuration.

[29] As shown in Figures 3b, 4b, and 5b, the upper layer flow velocity *U* appears to be a non monotonic function of Γ: first decreasing when Γ is small, then increasing when Γ is larger than about 0.3.

[30] The averaged measured data *Y* and *U* together with Γ are reported for all the experimental series in Tables 5–17.

[31] The relative submergence Y/D_s and the average Froude number, calculated with the mean flow velocity $\overline{U}$ and total flow depth *Y*, were in the range of 0.509–2.142 and 0.428–1.147 in the *Random pattern* case, respectively; between 0.465–3.505 and 0.358–2.748 for the *Transversal stripe pattern*, and between 0.628–2.080 and 0.677–1.262 for the *Longitudinal stripe pattern*.

Table 8. Measured Data for Random X and Random XI Experimental Series

Random X			Random XI		
Γ, –	*Y*, m	*U*, m/s	Γ, –	*Y*, m	*U*, m/s
0.000	0.027	0.749	0.000	0.027	0.742
0.029	0.032	0.662	0.122	0.059	0.508
0.061	0.037	0.590	0.244	0.066	0.451
0.122	0.046	0.520	0.366	0.073	0.420
0.183	0.051	0.503	0.488	0.076	0.435
0.244	0.055	0.525	0.610	0.078	0.462
0.305	0.058	0.537	0.732	0.079	0.486
0.366	0.060	0.548	0.854	0.079	0.480
0.427	0.061	0.572	1.000	0.080	0.524
0.488	0.062	0.575	–	–	–
0.549	0.064	0.571	–	–	–
0.610	0.064	0.585	–	–	–
0.671	0.065	0.547	–	–	–
0.732	0.066	0.590	–	–	–
0.793	0.066	0.591	–	–	–
0.854	0.066	0.589	–	–	–
0.915	0.066	0.620	–	–	–
1.000	0.065	0.637	–	–	–

Table 9. Measured Data for TrStripes I, TrStripes II, and TrStripes III Experimental Series

TrStripes I			TrStripes II			TrStripes III		
Γ, –	*Y*, m	*U*, m/s	Γ, –	*Y*, m	*U*, m/s	Γ, –	*Y*, m	*U*, m/s
0.000	0.027	0.749	0.000	0.035	0.600	0.000	0.050	0.831
0.079	0.044	0.547	0.089	0.065	0.413	0.089	0.077	0.556
0.092	0.048	0.530	0.125	0.065	0.370	0.127	0.079	0.607
0.116	0.050	0.524	0.142	0.066	0.386	0.163	0.085	0.533
0.147	0.052	0.508	0.161	0.061	0.375	0.236	0.085	0.591
0.175	0.053	0.492	0.231	0.069	0.435	0.303	0.088	0.580
0.221	0.054	0.490	0.303	0.073	0.390	0.428	0.088	0.620
0.283	0.054	0.535	0.440	0.071	0.490	1.000	0.084	0.711
0.436	0.053	0.625	1.000	0.071	0.501	-	-	-
1.000	0.057	0.635	-	-	-	-	-	-

4. Results

[32] The theoretical model here proposed is applied to all the experimental runs in order to obtain the space-time averaged schematic flow velocity profiles. The model requires as inputs bed slope, flow discharge, macro-roughness density, and arrangement, *Y* and *U*. Results about the lower layer thickness made dimensionless with the pebble size d/D_s, the drag shear stress to total shear stress ratio τ_d/τ_g, and the dimensionless Chezy coefficient *C* are hereafter presented. These quantities can be written as functions of spatial density Γ, bed slope *S*, and a dimensionless measure of the flow discharge *Q*. Since the main objective of the paper is to define the influence on flow resistance due to macro-roughness geometry in the following, the results are reported in terms of the spatial density Γ and for the three spatial arrangements investigated.

[33] The ratio between lower layer thickness *d* and pebble short diameter D_s is given for the three employed patterns in Figures 6a, 7a, and 8a. The lower layer thickness *d* is one of the more significant parameter involved in the two-layer model; it represents the height of the flow layer in which the drag force is dominant, and therefore, it can be considered as a measure of the displacement of the main flow induced by the roughness. According to various authors [e.g., *Bayazit*, 1976; *Jackson*, 1981; *Nikora et al.*, 2001; *Smart*

Table 10. Measured Data for TrStripes IV, TrStripes V, and TrStripes VI Experimental Series

TrStripes IV			TrStripes V			TrStripes VI		
Γ, –	*Y*, m	*U*, m/s	Γ, –	*Y*, m	*U*, m/s	Γ, –	*Y*, m	*U*, m/s
0.000	0.027	0.743	0.000	0.045	0.831	0.000	0.024	0.540
0.080	0.044	0.495	0.117	0.095	0.530	0.040	0.032	0.445
0.120	0.054	0.482	0.176	0.096	0.583	0.074	0.038	0.391
0.140	0.061	0.462	0.176	0.096	0.580	0.090	0.041	0.371
0.170	0.060	0.427	0.215	0.100	0.534	0.130	0.047	0.313
0.220	0.061	0.487	0.298	0.104	0.568	0.176	0.053	0.340
0.250	0.062	0.533	0.454	0.103	0.610	0.241	0.056	0.363
0.320	0.065	0.518	0.610	0.102	0.635	0.346	0.058	0.420
0.420	0.065	0.547	1.000	0.099	0.649	1.000	0.061	0.425
0.620	0.065	0.548	-	-	-	-	-	-
1.000	0.065	0.637	-	-	-	-	-	-

Table 11. Measured Data for TrStripes VII, TrStripes VIII, and TrStripes IX Experimental Series

TrStripes VII			TrStripes VIII			TrStripes IX		
Γ, –	*Y*, m	*U*, m/s	Γ, –	*Y*, m	*U*, m/s	Γ, –	*Y*, m	*U*, m/s
0.000	0.027	0.735	0.000	0.020	0.652	0.000	0.026	0.760
0.043	0.036	0.554	0.043	0.028	0.499	0.040	0.036	0.677
0.074	0.044	0.497	0.068	0.030	0.440	0.071	0.040	0.601
0.099	0.050	0.482	0.099	0.039	0.409	0.099	0.051	0.445
0.130	0.058	0.428	0.127	0.041	0.375	0.127	0.058	0.465
0.185	0.060	0.476	0.185	0.050	0.298	0.182	0.062	0.409
0.244	0.063	0.481	0.241	0.049	0.350	0.244	0.064	0.406
0.355	0.062	0.512	0.346	0.052	0.380	0.352	0.065	0.546
1.000	0.069	0.563	1.000	0.057	0.440	1.000	0.067	0.607

Table 13. Measured Data for TrStripes XIII, TrStripes XIV, and TrStripes XV Experimental Series

TrStripes XIII			TrStripes XIV			TrStripes XV		
Γ, –	*Y*, m	*U*, m/s	Γ, –	*Y*, m	*U*, m/s	Γ, –	*Y*, m	*U*, m/s
0.000	0.026	0.778	0.000	0.025	0.904	0.000	0.021	0.832
0.043	0.034	0.697	0.043	0.033	0.688	0.096	0.032	0.662
0.071	0.039	0.635	0.071	0.041	0.640	0.127	0.036	0.520
0.099	0.042	0.548	0.099	0.043	0.597	0.179	0.049	0.508
0.130	0.050	0.513	0.130	0.048	0.532	0.241	0.053	0.379
0.185	0.057	0.474	0.185	0.057	0.522	0.346	0.052	0.463
0.241	0.062	0.504	0.238	0.062	0.503	1.000	0.061	0.637
0.349	0.065	0.528	0.349	0.063	0.570	-	-	-
1.000	0.065	0.633	1.000	0.065	0.702	-	-	-

et al., 2002], d is a characteristics height of the roughness, the so-called displacement height, which defines the level above which the velocity profile follows a logarithmic distribution. Results show that d/D_s increases non-linearly with the spatial density until to reach a maximum when Γ is sufficiently high.

[34] In the case of *Random pattern*, d/D_s increases with a regular monotonic behavior to reach asymptotically the maximum value of about 0.8 when Γ is greater that about 0.8. A much less regular d/D_s behavior can be observed for the *Transversal stripe* and the *Longitudinal stripe pattern*; in the former, d/D_s reaches a near constant value already when Γ is above about 0.4, in the latter d/D_s seems to be constant for $\Gamma > 0.2$, although the lack of data for $\Gamma > 0.4$ renders the interpretation difficult. These results suggest that for low values of Γ, d is rather small, the hydrodynamic origin of the bed is in proximity of the granular layer, therefore the roughness height felt by the flow is comparable with the bed grain size, whereas for high values of Γ, the main flow is almost entirely displaced above the macro-roughness and the hydrodynamic origin of the bed is at a level about 0.2 D_s below the roughness top.

[35] In Figures 6b, 7b, and 8b, the drag shear stress to total shear stress ratio (τ_d/τ_g) is presented as a function of Γ. The results reveal a non-monotonic behavior of τ_d/τ_g; in particular first τ_d/τ_g rapidly increases with Γ until to reach a maximum of about 0.40 in the case of the *Random pattern* up to 0.90 in the case of the *Transversal stripe pattern* when Γ is in the range (0.20–0.40). In this condition, the surface shear stress to total shear stress ratio is minimum, suggesting that the drag around the roughness plays a primary role in the development of the flow resistance in this range of macro-roughness spatial density. A further increase of Γ produces a decreasing value in τ_d/τ_g until it reaches 0 when $\Gamma = 1$; in this condition, the total shear stress is entirely associated to the skin friction developed on the surface of the macro-roughness. *Gomez* [1993], studying flow resistance developed by plane armored gravel beds in the case of low values of Γ, found that τ_d/τ_g can be as high as 0.85.

[36] Figures 6c, 7c, and 8c show a non-monotonic behavior of dimensionless Chezy coefficient C as a function of Γ. In particular, C is maximum when the bed is free from the macro-roughness then, as Γ increases, C decreases until to reach a minimum (corresponding to maximum flow resistance, being C an estimation of channel *conductance*). A further increase of Γ produces an increase of C until to reach a quasi-asymptotic value which is invariably smaller than the initial value. Note that, not surprisingly, all the experimental series exhibit a minimum in C in the same spatial density range which maximizes the τ_d/τ_g ratio.

[37] As pointed out by *Morris and Wiggert* [1971] for flow in closed conduits and later by *Nowell and Church* [1979], at least three main different conditions may occur as spatial density increases:

[38] 1. *isolated roughness*: when the distance between elements is relatively "high" no wake interaction occurs. In such case, flow resistance is proportional to the number of elements;

[39] 2. *wake interference*: when the elements are sufficiently "close" together and the wake behind each element overlaps with the next element. In such case, flow resistance is no longer given by the sum of the single effects, since the vortex generation and dissipation phenomena associated with each wake will interfere with those of the adjacent elements.

[40] 3. *skimming*: when the roughness elements are spaced so closely as to form a more or less smooth

Table 12. Measured Data for TrStripes X, TrStripes XI, and TrStripes XII Experimental Series

TrStripes X			TrStripes XI			TrStripes XII		
Γ, –	*Y*, m	*U*, m/s	Γ, –	*Y*, m	*U*, m/s	Γ, –	*Y*, m	*U*, m/s
0.000	0.026	0.881	0.000	0.020	0.726	0.000	0.023	0.764
0.040	0.035	0.758	0.043	0.028	0.568	0.043	0.031	0.645
0.071	0.039	0.723	0.074	0.034	0.472	0.071	0.036	0.559
0.099	0.051	0.519	0.099	0.038	0.439	0.099	0.039	0.488
0.127	0.056	0.489	0.127	0.040	0.378	0.130	0.049	0.457
0.182	0.061	0.454	0.185	0.050	0.342	0.185	0.053	0.429
0.244	0.063	0.489	0.244	0.056	0.407	0.241	0.058	0.418
0.346	0.065	0.566	0.349	0.056	0.417	0.349	0.058	0.493
1.000	0.067	0.637	1.000	0.059	0.499	1.000	0.061	0.570

Table 14. Measured Data for TrStripes XVI, TrStripes XVII, and TrStripes XVIII Experimental Series

TrStripes XVI			TrStripes XVII			TrStripes XVIII		
Γ, –	*Y*, m	*U*, m/s	Γ, –	*Y*, m	*U*, m/s	Γ, –	*Y*, m	*U*, m/s
0.000	0.022	0.894	0.000	0.023	0.978	0.000	0.058	0.633
0.096	0.040	0.579	0.096	0.035	0.511	0.060	0.074	0.566
0.185	0.048	0.551	0.185	0.050	0.626	0.079	0.076	0.551
0.241	0.055	0.450	0.241	0.055	0.477	0.108	0.078	0.563
0.346	0.062	0.502	0.346	0.062	0.564	0.150	0.081	0.560
1.000	0.062	0.727	1.000	0.063	0.738	0.228	0.082	0.575
–	–	–	–	–	–	0.298	0.083	0.587
–	–	–	–	–	–	1.000	0.091	0.537

Table 15. Measured Data for TrStripes XIX and TrStripes XX Experimental Series

TrStripes XIX			TrStripes XX		
Γ, –	*Y*, m	*U*, m/s	Γ, –	*Y*, m	*U*, m/s
0.000	0.058	0.633	0.000	0.058	0.633
0.088	0.078	0.544	0.098	0.093	0.510
0.121	0.080	0.544	0.122	0.101	0.525
0.171	0.088	0.508	0.171	0.109	0.523
0.226	0.088	0.541	0.268	0.102	0.515
0.331	0.090	0.562	0.317	0.111	0.560
0.433	0.091	0.583	0.468	0.111	0.589
1.000	0.100	0.542	0.620	0.111	0.609
-	-	-	1.000	0.103	0.611

Table 17. Measured Data for LonStripes III and LonStripes IV Experimental Series

LonStripes III			LonStripes IV		
Γ, –	*Y*, m	*U*, m/s	Γ, –	*Y*, m	*U*, m/s
0.000	0.045	0.831	0.000	0.027	0.743
0.072	0.060	0.661	0.072	0.040	0.574
0.137	0.063	0.625	0.093	0.043	0.542
0.180	0.066	0.637	0.136	0.046	0.540
0.216	0.066	0.700	0.179	0.047	0.544
0.267	0.067	0.656	0.266	0.049	0.578
0.363	0.068	0.675	0.352	0.048	0.560
1.000	0.084	0.711	1.000	0.065	0.637

pseudo-wall composed of the element crests and the enclosed pockets of dead fluid. Within these pockets, there are stable vortices, unable to separate and commingle with the bulk flow because of the closeness of the downstream wall of the element.

[41] The minimum of C maybe related to the transition from a *isolated roughness* to a *wake interference* flow. The above results underline the fundamental role played by macro-roughness spatial density in the flow resistance development in the case of macro-scale roughness. Note that Figure 7c shows that the experimental series *TrStripes XVIII*, *TrStripes XIX*, and *TrStripes XX* develop a Chezy coefficient much greater than the other experimental series; this is due to relative low channel slope employed in these experiments which was 0.2% only, one order of magnitude smaller than in the other experimental series *TrStripes I-XVII*.

[42] Further results [*Canovaro*, 2005], not reported here, suggest that the channel slope and the flow discharge play a second order role on the qualitative relationships between d/D_s, τ_d/τ_g, C, and Γ in particular the value of the spatial density range maximizing flow resistance is not affected neither by the slope nor by the flow discharge. These findings, although very consistent in the narrow discharge range employed, require further investigations as higher flow discharges may affect the value of the spatial density associated to the minimum of the flow resistance; in particular, it appears reasonable that at high relative submergence the influence of the spatial density becomes vanishing.

[43] A comparison among the employed patterns (*Random*, *Transversal stripes*, and *Longitudinal stripes*) for the runs with the same flow discharge, bed slope, and pebble size is reported in Figures 9a, 9b, and 9c. It appears that the behavior of *Random pattern* is intermediate between *Transversal stripe pattern* and *Longitudinal stripe pattern*. For low values of Γ, the influence played by the patterns seems to be negligible, probably due to fact that wakes forming around the roughness are non-interfering. The influence of the patterns seems to be more evident for the Γ values maximizing flow resistance. In particular, it appears that *Transversal stripe pattern* is the more dissipative arrangement, whereas the minimum drag shear stress is associated with the *Longitudinal stripe pattern* (in the constant spatial density case). This result is very much reasonable, since in the case of *Transversal stripe pattern*, the major part of the flow impacts on the stripes, whereas in case of *Longitudinal stripe pattern*, flow is funneled among the stripes.

Table 16. Measured Data for LonStripes I and LonStripes II Experimental Series

LonStripes I			LonStripes II		
Γ, –	*Y*, m	*U*, m/s	Γ, –	*Y*, m	*U*, m/s
0.000	0.027	0.749	0.000	0.034	0.595
0.024	0.031	0.692	0.050	0.048	0.532
0.031	0.031	0.670	0.094	0.053	0.552
0.045	0.032	0.639	0.159	0.055	0.525
0.059	0.033	0.639	0.180	0.056	0.544
0.088	0.036	0.597	0.238	0.056	0.503
0.116	0.034	0.609	0.310	0.058	0.521
0.154	0.036	0.614	0.358	0.056	0.553
1.000	0.054	0.635	1.000	0.071	0.501

5. Discussion

[44] Comparison between the present results and data from other authors is here reported for the *Random pattern* (Figures 10 and 11) and the *Transversal stripe pattern* (Figures 12, 13 and 14).

[45] In Figure 10, d/D_s is compared with *Counihan* [1971] and *Lee and Soliman* [1977] data, obtained from wind-tunnel experiments. Notwithstanding the existing differences among the experiments, the comparison is quite good, indicating that d/D_s is able to describe the effects of the macro-roughness on the displacement of the main flow for different types of fluids. Moreover, note that the maximum value reached by d/D_s (around 0.8) for $\Gamma = 1$ is in agreement with the finding of *Bayazit* [1976], who proposed $d/D_s = 0.8$ as the mean log-law profile displacement in case of a bed fully covered by macro-roughness elements.

[46] In Figure 11, the equivalent roughness size K_s, estimated by means of the well-known Keulegan flow resistance law and made dimensionless with D_s, is compared with the data of *Schlichting* [1936]; *O'Loughlin and Macdonald* [1964]; and *Koloseus and Davidian* [1966], who performed experiments on a smooth bed with schematic macro-roughness elements. It appears that K_s/D_s attains a non-monotonic behavior and shows a maximum for the usual Γ range (0.2–0.4); this maximum can be as high as 4. The experimental series which show the larger values of K_s/D_s (*Random III*, *IX-XI*) are those associated to either high bed slopes or large pebble size (*Random XI*) or low flow discharge. The comparison with the other authors' data is encouraging, showing that for the same Γ range a maximum

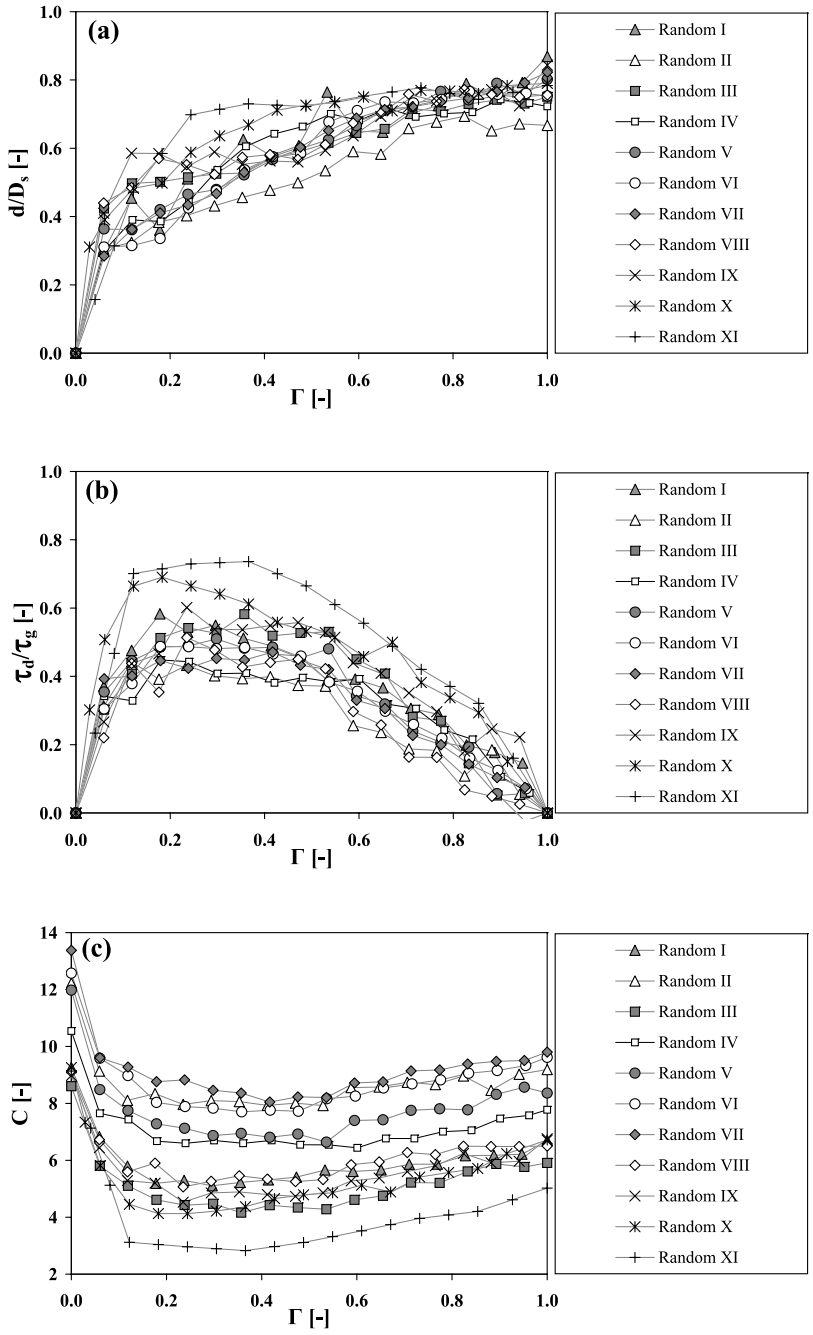

Figure 6. (a) Lower layer thickness to pebble short diameter ratio (d/D_s), (b) drag shear stress to total shear stress ratio (τ_d/τ_g), and (c) dimensionless Chezy coefficient (C) as functions of spatial density (Γ), in the case of *Random pattern*.

in flow resistance is developed by all the different macro-roughness arrangements.

[47] With regard to *Transversal stripe pattern*, the results here presented, for the experimental runs *TrStripes I-XVII* for relative high bed slopes, appear to be in agreement with those obtained by *Johnson and LeRoux* [1946] and *Wohl and Ikeda* [1998] in the case of experiments on schematic macro-roughness elements represented by transversal ribs positioned according to a regularly spaced-stripe pattern. The comparisons with the latter authors are reported in Figures 12 and 13 for C and K_s/D_s as a function of D_s/λ. It appears that when D_s/λ is ranging between 0.1 and 0.2, flow resistance is maximum. The experiments *TrStripes XVIII-XX*, characterized by relative low bed slopes, are compared in Figure 14 with the data obtained by *Pillai* [1979] in case of experiments on a channel bed covered with fixed dune-shaped undulations. Note that also in this case, the agreement is fairly good at least in the range of low values of D_s/λ taken into account.

[48] A further issue which needs to be investigated is about the possible extension of the present results obtained in the case of artificial macro-roughness patterns to the case of flows over macro-roughness in the field. Notwithstanding that employed patterns are only a schematic representation

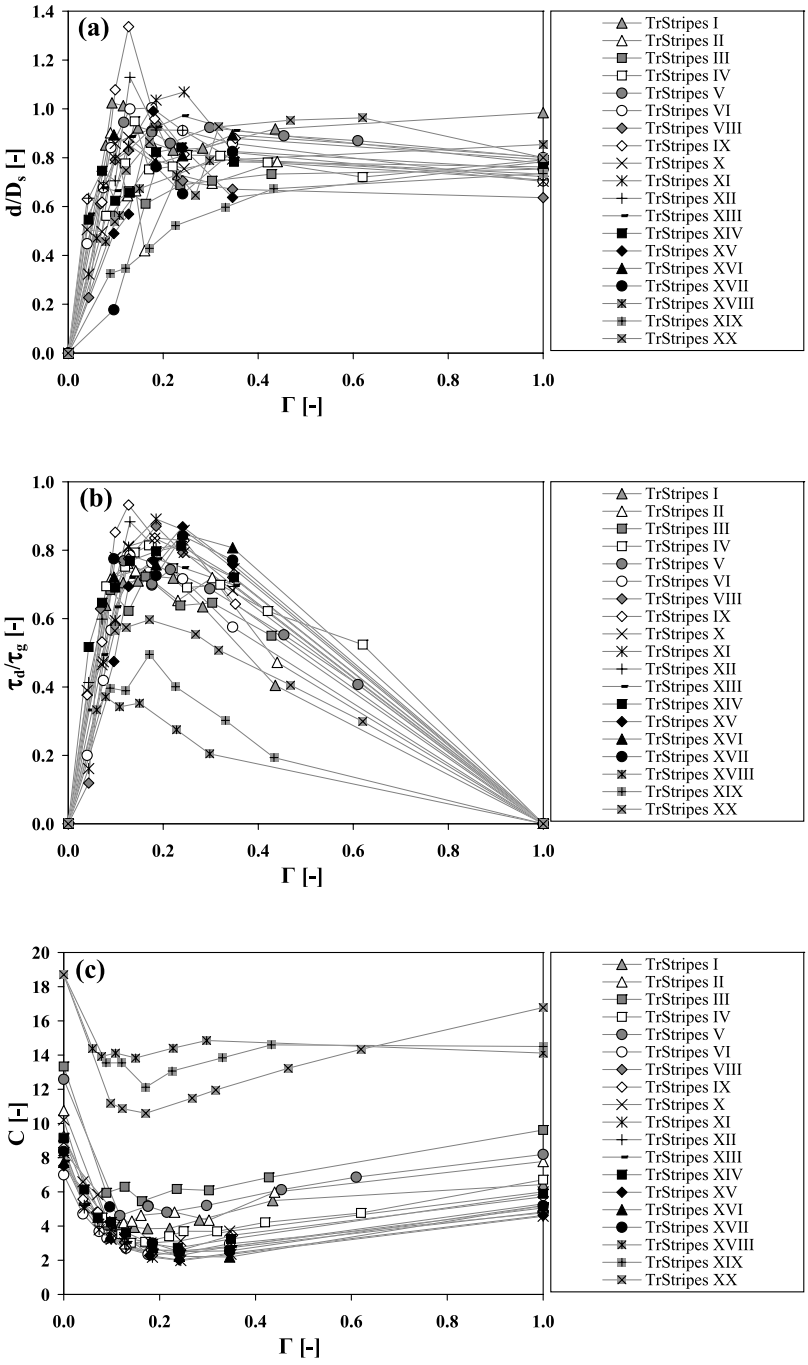

Figure 7. (a) Lower layer thickness to pebble short diameter ratio (d/D_s), (b) drag shear stress to total shear stress ratio (τ_d/τ_g), and (c) dimensionless Chezy coefficient (C) as functions of spatial density (Γ), in the case of *Transversal stripe pattern*.

of natural configurations, it seems reasonable to observe some general parallels between flow resistance in natural rivers and the present flume results. In particular, *Random pattern* may be associated with the random disposition of the boulders in steep-mountain streams [*Nikora et al.*, 1998]. Moreover, the range of the employed flume bed slopes (0.005–0.025), the low relative submergences ($Y/D_s < 5$), and the values of the equivalent roughness height K_s on the order of the large clast size D_s suggest that the geometric and hydraulic experimental conditions are comparable to those that can be commonly observed in natural steep-mountain streams [e.g., *Bathurst*, 1985; *Wiberg and Smith*, 1991].

[49] The experiments (I-XVIII) of *Transversal stripe pattern* may be regarded as a rough representation of step-pool sequences: the bed slopes taken into account (0.01–0.06) are in the step-pool forming range [*Montgomery and Buffington*, 1997] and the dimensionless spacing between the stripes, $D_s/\lambda \approx 0.1–0.2$, maximizing flow resistance appears to be to most frequent observed in nature [e.g.,

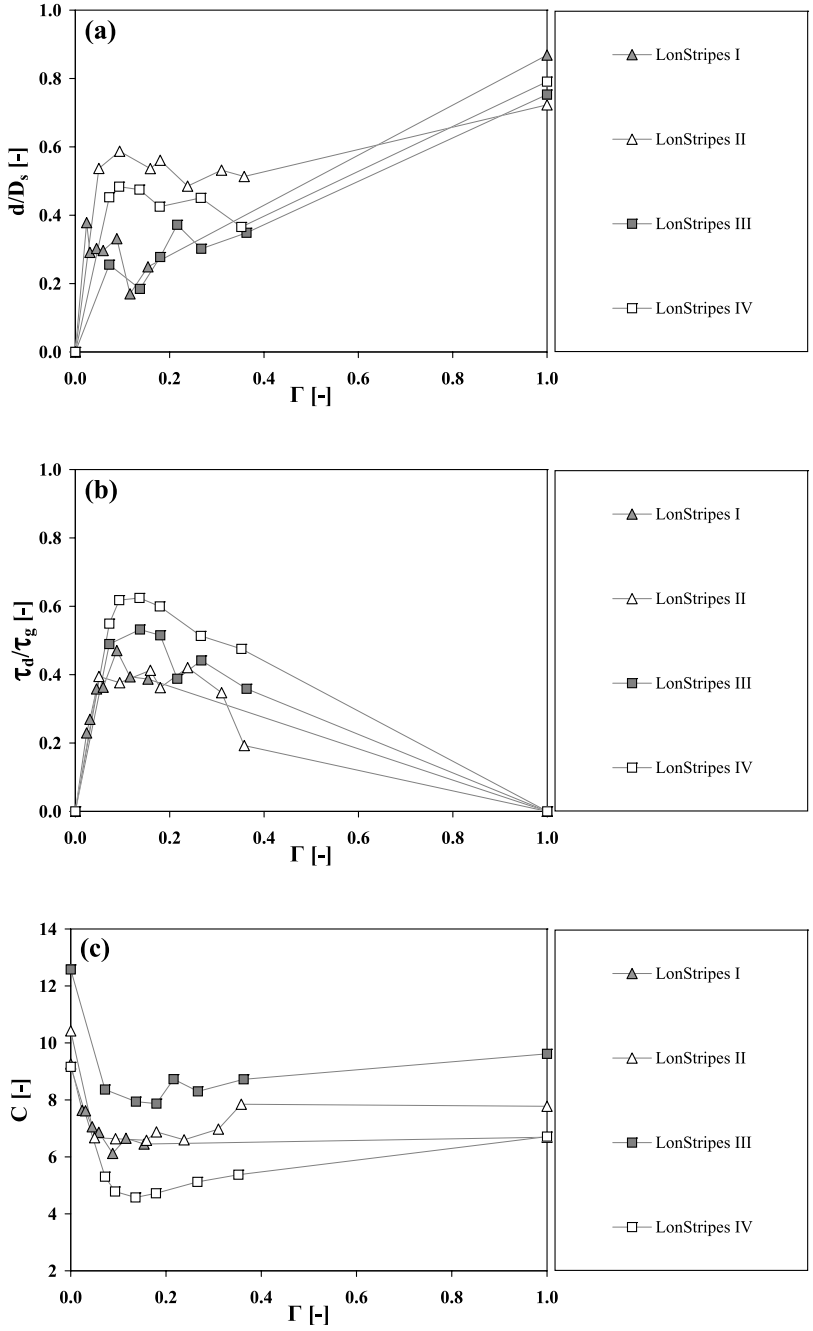

Figure 8. (a) Lower layer thickness to pebble short diameter ratio (d/D_s), (b) drag shear stress to total shear stress ratio (τ_d/τ_g), and (c) dimensionless Chezy coefficient (C) as functions of spatial density (Γ), in the case of *Longitudinal stripe pattern*.

Chin, 1999; *Chartrand and Whiting*, 2000; *Curran and Wilcock*, 2005].

[50] A specific application of the present theoretical model to the *Transversal stripe pattern* with the main aim to find analogies between the dissipative behavior of real step-pool sequences and the present laboratory schematic pattern can be found in the study of *Canovaro and Solari* [2007].

[51] The experiments (XVIII-XX) of *Transversal stripe pattern* carried out with a relative low bed slope (0.002) and with a dimensionless spacing around 0.1 seems to recall a dune-covered bed [e.g., *Vanoni and Hwang*, 1967; *Yalin and Karahan*, 1979].

6. Conclusions

[52] In the present work, a theoretical model and laboratory experiments devoted to investigate the average flow field of a free surface flow over macro-roughness elements are proposed.

[53] Results show that the geometry of the macro-roughness in terms of spatial density and planimetric arrangement plays a primary role in the development of the flow

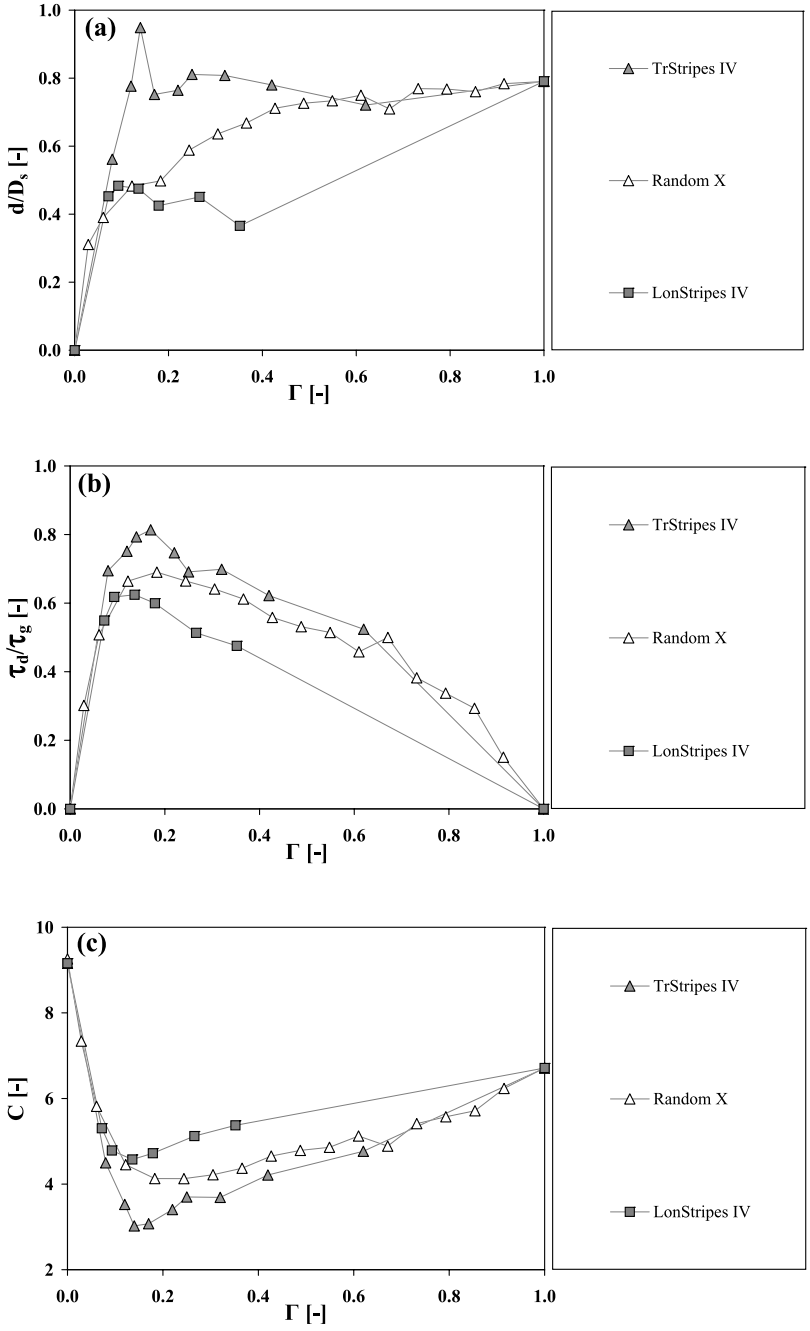

Figure 9. Comparison among lower layer thickness to pebble short diameter ratio (d/D_s) (a), drag shear stress to total shear stress ratio (τ_d/τ_g), (b) and dimensionless Chezy coefficient (C) (c) developed by the employed patterns.

resistance. In particular, it appears that when the spatial density is in the range between 0.20 and 0.40, the ratio of drag shear stress developed around the macro-roughness to total bed shear stress is maximum with values that can be as high as 0.90, thus suggesting that in these conditions, the flow resistance is mainly associated to form friction mechanism, whereas the skin friction plays a relative minor role. In the same range of spatial density flow resistance is maximum, the Chezy coefficient being smaller in both cases of bed with no macro-roughness and bed fully covered by the macro-roughness.

[54] The macro-roughness planimetric arrangement is also able to influence flow field: results show that *Transversal stripe pattern* is the most dissipative arrangement among those investigated, *Longitudinal stripe pattern* develops the lowest dissipation, and the *Random pattern* shows an intermediate behavior. The influence of the planimetric arrangement is, however, such not to modify the values of the spatial density for which flow resistance is maximum.

[55] The above findings suggest that the classical flow resistance formulae developed for low-land rivers cannot be

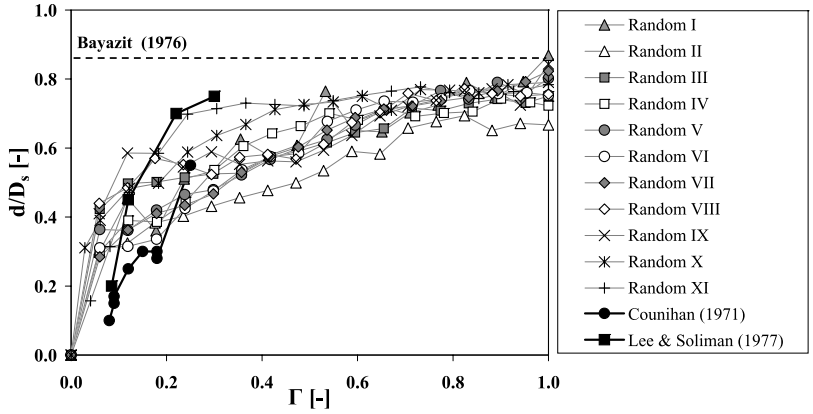

Figure 10. Comparison between dimensionless lower layer thickness (d/D_s) obtained in this study and that obtained by other authors.

applied to describe the flow resistance in the presence of macro-roughness such as in steep mountain rivers; future developments of the present work are needed in order to find a predictive relationship able to take into account all the parameters in the evaluation of the flow resistance.

Appendix A: Method of Calculation for the Reduction Factor ψ

[56] As previously outlined, the reduction factor is defined as the ratio between the cross-sectional area occupied by the flow among the macro-roughness elements in the lower layer and the total cross-sectional area of the lower layer. According to this definition, the reduction factor can be written as follows:

$$\psi = \frac{A_{ll} - A_{llp}}{A_{ll}} = 1 - \frac{A_{llp}}{A_{ll}} \tag{A1}$$

where A_{ll} is the total cross-sectional area of the lower layer, and A_{llp} is the pebble cross-sectional area in the lower layer. The pebbles have an ellipsoidal shape and are oriented with the short axis D_s perpendicular to the bed and the intermediate axis D_m perpendicular to the channel axis. Taking into account a bed area of unit width, A_{ll} is evaluated as follows:

$$A_{ll} = d \cdot 1 \tag{A2}$$

[57] The value of A_{llp} is a function of the type of the planimetric arrangement, as it is shown in the following.

A1. Random Pattern

[58] In this case, A_{llp} is evaluated as follows:

$$A_{llp} = \begin{cases} \sqrt{N_u} \cdot \frac{\pi}{4} D_s D_m & \text{if } d < D_s \\ \sqrt{N_u} \cdot \frac{\pi}{4} d D_m & \text{if } d > D_s. \end{cases} \tag{A3}$$

[59] Substituting from equation A3 into equations A1 and A2, the reduction factor is obtained:

$$\psi = \begin{cases} 1 - \frac{\pi}{4} D_m \sqrt{N_u} & \text{if } d \le D_s \\ 1 - \frac{\pi}{4} \frac{D_s}{d} D_m \sqrt{N_u} & \text{if } d > D_s. \end{cases} \tag{A4}$$

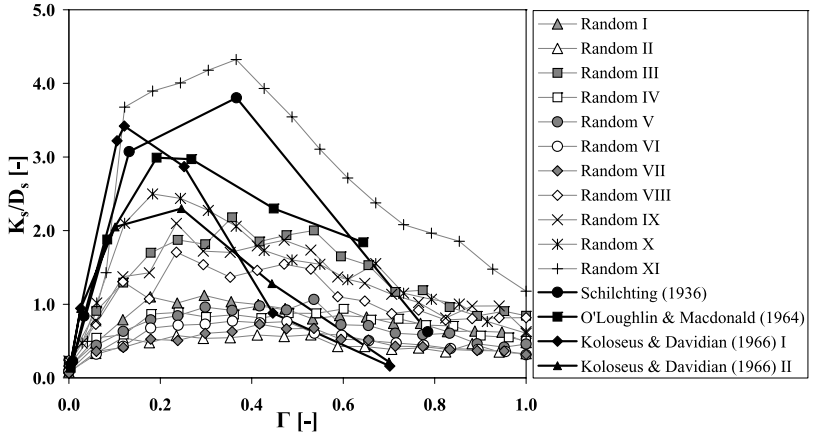

Figure 11. Comparison between dimensionless equivalent roughness dimension (K_s/D_s) obtained in this study and that obtained by other authors.

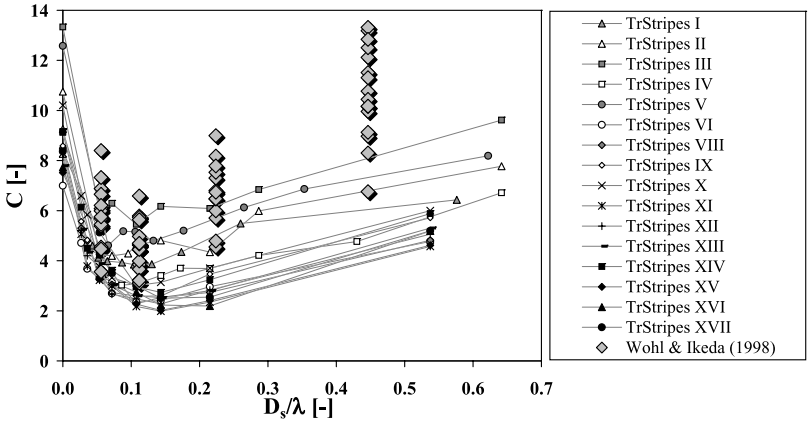

Figure 12. Comparison with *Wohl and Ikeda* [1998] experiments.

[60] The number of pebbles arranged on a unit bed area N_u can be expressed as a function of the spatial density Γ, being:

$$N_u = N_u^{max} \cdot \Gamma = \frac{4}{\pi}\frac{1\cdot 1}{D_m D_l}\cdot \Gamma \Rightarrow N_u = \frac{4}{\pi}\frac{\Gamma}{D_m D_l} \tag{A5}$$

Combining equations A5 and A4, a definition of ψ as a function of Γ is obtained:

$$\psi = \begin{cases} 1 - \sqrt{\frac{\pi}{4}\frac{D_m}{D_l}\Gamma} & \text{if } d \le D_s \\ 1 - \sqrt{\frac{\pi}{4}\frac{D_s^2 D_m}{d^2 D_l}\Gamma} & \text{if } d > D_s. \end{cases} \tag{A6}$$

A2. Transversal Stripe Pattern

[61] The pebble cross-sectional area in the lower layer A_{llp} is estimated with the following:

$$A_{llp} = \begin{cases} \left[\left(\frac{\pi}{4}dD_m\right)\cdot\left(\frac{4}{\pi}\frac{D_l}{D_m D_l}\right)\cdot D_l\right]\cdot\frac{1}{\lambda} = d\frac{D_l}{\lambda} & \text{if } d \le D_s \\ \left[\left(\frac{\pi}{4}D_s D_m\right)\cdot\left(\frac{4}{\pi}\frac{D_l}{D_m D_l}\right)\cdot D_l\right]\cdot\frac{1}{\lambda} = D_s\frac{D_l}{\lambda} & \text{if } d > D_s. \end{cases} \tag{A7}$$

[62] Hence the reduction factor ψ reads as follows:

$$\psi = \begin{cases} 1 - \frac{D_l}{\lambda} & \text{if } d \le D_s \\ 1 - \frac{D_s}{d}\frac{D_l}{\lambda} & \text{if } d > D_s. \end{cases} \tag{A8}$$

[63] Evaluating the spatial density $\Gamma = N_\lambda / N_\lambda^{max}$, where N_λ and N_λ^{max} are the actual number and the maximum number of pebbles arranged on a bed area $1\cdot\lambda$, respectively, and are defined as follows:

$$N_\lambda = D_l \cdot 1 \cdot \left(\frac{4}{\pi}\frac{1}{D_m D_l}\right) = \frac{4}{\pi}\frac{1}{D_m} \tag{A9}$$

$$N_\lambda^{max} = \lambda \cdot 1 \cdot \left(\frac{4}{\pi}\frac{1}{D_m D_l}\right) = \frac{4}{\pi}\frac{\lambda}{D_m D_l} \tag{A10}$$

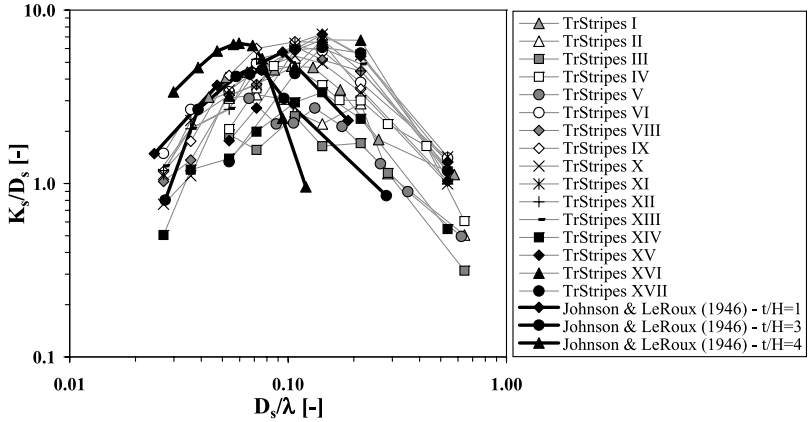

Figure 13. Comparison with *Johnson and LeRoux* [1946] experiments, in case of *Transversal stripe pattern*. Experimental series here shown correspond to a t/H ratio around 2, with t corresponding to D_l and H corresponding to D_s.

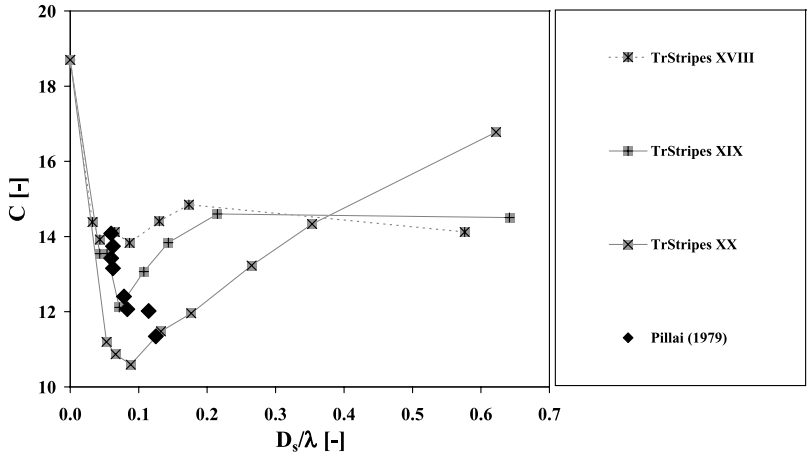

Figure 14. Chezy coefficient as a function of D_s/λ ratio compared to *Pillai* [1979] experiments.

one can obtain the relationship:

$$\Gamma = \frac{D_l}{\lambda} \tag{A11}$$

[64] Combining A8 with A11, the reduction factor ψ can be expressed as a function spatial density:

$$\psi = \begin{cases} 1-\Gamma & \text{if } d \le D_s \\ 1-\dfrac{D_s}{d}\Gamma & \text{if } d > D_s. \end{cases} \tag{A12}$$

A3. Longitudinal Stripe Pattern

[65] A_{llp} is in this case defined as follows:

$$A_{llp} = \begin{cases} \left[\left(\dfrac{\pi}{4}dD_m\right)\cdot N_r \cdot D_l\right]\cdot\dfrac{1}{\lambda} = \dfrac{\pi}{4}dD_m N_r \dfrac{D_l}{\lambda} & \text{if } d \le D_s \\ \left[\left(\dfrac{\pi}{4}D_s D_m\right)\cdot N_r \cdot D_l\right]\cdot\dfrac{1}{\lambda} = \dfrac{\pi}{4}D_s D_m N_r \dfrac{D_l}{\lambda} & \text{if } d > D_s. \end{cases} \tag{A13}$$

where N_r is the number of longitudinal stripes.

[66] Substituting from equation A8 into A1, the following expression for the reduction factor is obtained:

$$\psi = \begin{cases} 1-\dfrac{\pi}{4}D_m N_r \dfrac{D_l}{\lambda} & \text{if } d \le D_s \\ 1-\dfrac{\pi}{4}\dfrac{D_s}{d}D_m N_r \dfrac{D_l}{\lambda} & \text{if } d > D_s. \end{cases} \tag{A14}$$

[67] The reduction factor can be also defined in terms of spatial density. Defining $\Gamma = N_\lambda/N_\lambda^{max}$ with $N_\lambda = N_r$ and taking into account equation A10, Γ can be expressed as:

$$\Gamma = N_r \cdot \frac{\pi}{4}\frac{D_m D_l}{\lambda} \tag{A15}$$

[68] Finally, ψ reads as follows:

$$\psi = \begin{cases} 1-\Gamma & \text{if } d \le D_s \\ 1-\dfrac{D_s}{d}\Gamma & \text{if } d > D_s. \end{cases} \tag{A16}$$

Appendix B: Method of Calculation for the Streamwise Water Mass Weight Component

[69] Considering an unitary bed area, the total bed shear stress is defined as $\tau_g = F_g/(1\cdot1)$, where F_g is the streamwise water mass weight component. F_g is a function of the actual water volume contained in the control volume of height Y and reads as follows:

$$F_g = \rho g S(V - V_p) \tag{B1}$$

where V is the total control volume, and V_p is the pebble volume, with

$$V = Y \cdot 1 \cdot 1 \tag{B2}$$

and

$$V_p = \frac{4\pi}{3}\cdot\left(\frac{D_s D_m D_l}{8}\right)\cdot N_u \tag{B3}$$

Assuming that pebbles can be approximated with ellipsoids with D_l the long axis, D_m the intermediate axis and D_s the short axis. N_u is estimated as follows:

$$N_u = \Gamma N_u^{max} = \Gamma\cdot\left(\frac{4}{\pi}\cdot\frac{1\cdot1}{D_m D_l}\right) \tag{B4}$$

[70] Combining equations B1, B2, B3, and B4, the streamwise water mass weight component is obtained:

$$F_g = \rho g S Y\left(1-\frac{2}{3}\frac{D_s}{Y}\Gamma\right) \tag{B5}$$

[71] **Acknowledgments.** The CERAFRI (Centre of Research and Advanced Education for Hydrogeological Risk Prevention) is kindly acknowledged for its assistance. The authors wish also to thank Elena Facchini, Lorenzo Minatti, Irene Morganti, and Luca Nelli, who have carried out a part of experimental activity herein presented. The authors are

also grateful to Robert Ferguson and two anonymous reviewers for their helpful comments.

References

Aberle, J., and G. M. Smart (2003), The influence of roughness structure on flow resistance on steep slopes, *J. Hydraul. Res.*, *41*(3), 259–269.

Aguirre-Pe, J., and R. Fuentes (1990), Resistance to flow in steep rough streams, *J. Hydraul. Eng.*, *116*(11), 1374–1387.

Baiamonte, G., G. Giordano, and V. Ferro (1995), Advances on velocity profile and flow resistance law in gravel bed rivers, *Excerpta*, *9*, 41–89.

Bathurst, J. C. (1985), Flow resistance estimation in mountain rivers, *J. Hydraul. Eng.*, *111*(4), 625–643.

Bathurst, J. C. (1987), Flow resistance estimation in mountain rivers-closure, *J. Hydraul. Eng.*, *113*(6), 822–824.

Bathurst, J. C. (1996), Field measurements of boulder flow drag, *J. Hydraul. Eng.*, *122*(3), 167–169.

Bathurst, J. C., R. M. Li, and D. B. Simons (1981), Resistance equation for large-scale roughness, *J. Hydraul. Eng.*, *111*(12), 1593–1613.

Bayazit, M. (1976), Surface flow in a channel of large relative roughness, *J. Hydraul. Res.*, *14*(2), 115–125.

Bettess, R. (1999), Flow resistance for gravel bed rivers, Proceedings of XXVIII IAHR Congress, Graz, Austria, August 22–27.

Canovaro, F. (2005), Flow resistance of macro-scale roughness, PhD thesis, Civil Engineering Department, Firenze University, Via Santa Marta 3, 50139 Firenze, Italy.

Canovaro, F., and L. Solari (2007), Dissipative analogies between a schematic macro-roughness arrangement and step-pool morphology, *Earth Surf. Processes Landforms*, in press.

Carollo, F. G., V. Ferro, and D. Termini (2002), Flow velocity measurements in vegetated channels, *J. Hydraul. Eng.*, *128*(7), 664–673.

Chartrand, S. M., and P. J. Whiting (2000), Alluvial architecture in headwater streams with special emphasis on step-pool topography, *Earth Surf. Processes Landforms*, *25*, 583–600.

Chin, A. (1999), The morphologic structure of step-pools in mountain streams, *Geomorphology*, *27*(3-4), 191–204.

Colosimo, V., A. Copertino, and M. Veltri (1988), Friction factor evaluation in gravel bed rivers, *J. Hydraul. Eng.*, *114*(8), 771–778.

Counihan, J. (1971), Wind tunnel determination of the roughness length as a function of the fetch and the roughness of three dimensional elements, *Atmos. Environ.*, *5*, 637–642.

Curran, J. C., and P. R. Wilcock (2005), Characteristic dimensions of the step-pool bed configuration: An experimental study, *Water Resour.*, 41.

Ferro, V. (1999), Friction factor for gravel bed channel with high boulder concentration, *J. Hydraul. Eng.*, *125*(7), 771–778.

Ferro, V., and G. Giordano (1993), Velocity profile and flow resistance in gravel bed rivers, *Excerpta*, *7*, 99–144.

Gomez, B. (1993), Roughness of stable, armored gravel beds, *Water Resour. Res.*, *29*(11), 3631–3642.

Graf, W. H. (1984), Flow resistance for steep, mobile channels, Workshop on "Idraulica del territorio montano", Bressanone, Italy.

Hey, R. D. (1979), Flow resistance in gravel bed rivers, *J. Hydraul. Div.*, *105*, 365–379.

Jackson, P. S. (1981), On the displacement height in the logarithmic velocity profile, *J. Fluid Mech.*, *111*, 15–25.

Järvelä, J. (2002), Determination of flow resistance of vegetated channel banks and floodplain', Proceedings of River Flow 2002, Louvain-La-Neuve (Belgium), September 4–6, 1, 311–318.

Johnson, J. W., and E. A. LeRoux (1946), Discussion of powell r. w. "flow in a channel of definite roughness", *Trans. ASCE*, *111*, 531–566.

Katul, G., P. Wiberg, J. Albertson, and G. Hornberger (2002), A mixing layer theory for flow resistance in shallow streams, *Water Resour. Res.*, *38*(11), 1250, doi:10.1029/2001WR000817.

Koloseus, H., and J. Davidian (1966), Roughness concentration effects on flow over hydrodynamically rough surfaces, USGS Water Supply Paper No. 1592-D.

Lawrence, D. S. (2000), Hydraulic resistance in overland flow during partial and marginal surface inundation: Experimental observations and modeling', *Water Resour. Res.*, *36*(8), 2381–2393.

Lee, B. E., and B. F. Soliman (1977), An investigation of the forces on three-dimensional bluff bodies in rough wall turbulent boundary layers, *J. Fluid Eng.*, *99*, 503–510.

Marchand, J. P., R. D. Jarrett, and L. L. Jones (1984), Velocity profile, water-surface slope, and bed-material size for selected streams in Colorado, U.S.G.S. Open File Report, 84-733, 82 p.

Montgomery, D. R., and J. M. Buffington (1997), Channel-reach morphology in mountain drainage basins, *Geol. Soc. Am. Bull.*, *109*(5), 596–611.

Morris, H. M., and J. M. Wiggert (1971), Applied hydraulics in engineering, John Wiley and Sons, Inc., New York, USA.

Nikora, V. I., D. G. Goring, and B. J. F. Biggs (1998), On gravel bed roughness characterization, *Water Resour. Res.*, *34*(3), 517–527.

Nikora, V. I., D. G. Goring, I. McEwan, and G. Griffiths (2001), Spatially average open-channel flow over rough bed, *J. Hydraul. Eng.*, *127*(2), 123–133.

Nowell, A. R. M., and M. Church (1979), Turbulent flow in a depth-limited boundary layer, *J. Geophys. Res.*, *84*, 4816–4824.

O'Loughlin, E., and B. Macdonald (1964), Some roughness-concentration effects on boundary resistance, *La Houille*, 7.

Pillai, C. (1979), Effective depth in channels having bed undulations, *J. Hydraul. Div., ASCE*, *1*, 67–81.

Pyle, R., and P. Novak (1981), Coefficient of friction in conduits with large roughness, *J. Hydraul. Res.*, *19*(2), 119–139.

Roberson, J. A., M. Bajwa, and S. J. Wright (1974), A general theory for flow in rough conduits, *J. Hydraul. Eng.*, *12*(2), 223–240.

Rouse, H. (1965), Critical analysis of open channel resistance, *J. Hydraul. Div.*, *91*(4), 1–25.

Schlichting, H. (1936), Experimentelle untersuchungen zum rauhigkeitsproblem, *Ingenieur Archiv*, *7*, 1–34.

Smart, G. M., M. J. Duncan, and J. Walsh (2002), Relatively rough flow resistance equations, *J. Hydraul. Eng.*, *128*(6), 568–578.

Stone, B. M., and H. T. Shen (2002), Hydraulic resistance of flow in channels with cylindrical roughness, *J. Hydraul. Eng.*, *128*(5), 500–506.

Vanoni, V. A., and L. S. Hwang (1967), Relation between bed forms and friction in streams, *J. Hydraul. Div., ASCE*, *93*(5), 121–144.

Wiberg, P. L., and J. D. Smith (1991), Velocity distribution and bed roughness in high-gradient streams, *Water Resour. Res.*, *27*(5), 825–838.

Wohl, E. E., and H. Ikeda (1998), The effect of roughness configuration on velocity profiles in an artificial channel, *Earth Surf. Processes Landforms*, *23*, 159–169.

Yalin, M. S., and E. Karahan (1979), Steepness of sedimentary dunes, *J. Hydraul. Div., ASCE*, *105*(4), 381–392.

Zimmermann, A., and M. Church (2001), Channel morphology, gradient profiles and bed stresses during flood in step-pool channel, *Geomorphology*, *40*(3-4), 311–327.

F. Canovaro, CERAFRI (Centre of Research and Advanced education for Hydrogeological Risk Prevention), Via 11 Febbraio 2, 55040, Retignano di Stazzema (LU), Italy. (francesco.canovaro@cerafri.it; francesco.canovaro@dicea.unifi.it)

E. Paris and L. Solari, Department of Civil and Environmental Engineering, University of Firenze, Via Santa Marta 3, 50139, Firenze, Italy. (eparis@dicea.unifi.it; luca.solari@dicea.unifi.it)